BJRS
BRAZILIAN JOURNAL OF RADIATION SCIENCES

doi.org/10.15392/2319-0612.2026.3014
Braz. J. Radiat. Sci., Rio de Janeiro
2026, 14(1) | 01-30| e3014
Editor: Prof. Dr. Bernardo Maranhão Dantas
Editor: Prof. Dr. Alfredo Lopes Ferreira Filho
Submitted: 2025-10-09
Accepted: 2026-01-29

Original Article

Advances of the Modified Spectral Deterministic method applied in the solution of two-dimensional neutron shielding problems considering linearly anisotropic scattering

Libotte[a*], R. B.; Alves Filho[a], H.; Silva, F. C.[b]

[a]Instuto Politécnico - UERJ, 28.625-570, Nova Friburgo, Rio de Janeiro, Brazil.
[b]Universidade Federal do Rio de Janeiro, 21941-901, Rio de Janeiro, Rio de Janeiro, Brazil

*Correspondence: rafaellibotte@hotmail.com

Abstract: This work extends the application of the spectral-nodal method SDM, cf., Modified Spectral Deterministics (MSD-CN), to solve neutron shielding problems (fixed-source) in two-dimensional Cartesian rectangular geometry, considering problems with linearly anisotropic scattering in the formulation of discrete ordinates (S_N), using a constant approximation for the transverse neutron leakage terms. The essence of this methodology lies in the use of the intranodal analytical solution of the neutron transport equation and an iterative process that employs the concept of spatial sweeping, like the Source Iteration method used in the fine-mesh method DD, cf., Diamond Difference, for estimating the angular neutron fluxes emerging in the spatial nodes. To validate the methodology, a numerical simulation of two model-problems was performed, where the MSD-CN was able to achieve numerical results with a small relative deviation compared to the reference method Diamond Difference alongside a performance test to compute the execution time of the algorithm. All methods were implemented in the computational language C++.

Keywords: Neutron transport theory, spectral-nodal methods, Computational neutronics, linearly anisotropic scattering.

doi.org/10.15392/2319-0612.2026.3014
Braz. J. Radiat. Sci., Rio de Janeiro
2026, 14(1) | 01-30| e3014
Editor: Prof. Dr. Bernardo Maranhão Dantas
Editor: Prof. Dr. Alfredo Lopes Ferreira Filho
Submitted: 2025-10-09
Accepted: 2026-01-29

Avanços do Modified Spectral Deterministic aplicado à solução de problemas bidimensional de blindagem de nêutrons considerando espalhamento linearmente anisotrópico

Resumo: Este trabalho amplia a aplicação do método espectro-nodal MSD. cf., Modified Spectral Deterministics (MSD-CN) para resolver problemas de blindagem de nêutrons (fonte fixa) em geometria retangular cartesiana bidimensional, considerando problemas com espalhamento linearmente anisotrópico, na formulação das ordenadas discretas (S_N), usando aproximação constante para os termos de fuga transversal de nêutrons. O fundamental dessa metodologia é a utilização da solução analítica intranodal da equação de transporte de nêutrons e um processo iterativo que emprega o conceito de varredura espacial, semelhante a do método SI, c.f., Source Iteration, utilizado no método de malha fina DD, cf., Diamond Difference para a estimativa dos fluxos angulares de nêutrons emergentes nos nodos espaciais. Para a validação da metodologia, foi feita a simulação numérica de dois problemas-modelo, onde o MSD-CN foi capaz de gerar resultados com baixo desvio em relação aos obtidos usando o método de malha fina de referência, em conjunto com um teste de desempenho onde o tempo de exeução do algoritmo foi testado. Diamond Difference. Todos os métodos foram implementados em C++.

Palavras-chave: Teoria de transporte de nêutrons, métodos espectro-nodais, neutrônica computacional, espalhamento linearmente anisotrópico.

1. INTRODUCTION

Obtaining an analytical solution for integro-differential equation systems has always been a challenging task. Since neutron transport problems are modelled in this way [10], the use of numerical methods provides a viable solution for solving neutron shielding problems. Over the years, methods with different approaches were developed in order to solve these problems, stochastic methods, using the Monte Carlo method [21], and deterministic methods, such as the fine-mesh method Diamond Difference (DD) [12], which is used as the reference method in this work. Coarse-mesh methods such as the spectral Green's function (SGF) [4, 5, 6], Spectral Deterministic Method (SDM) [16, 17], Response Matrix (RM) [9, 20] and Analytical Discrete Ordinates (ADO) [1, 2, 3], are largely studied, once they deliver numerical results with no spatial truncation error in one-dimensional problems, and can solve multidimensional problems with coarser meshes, when compared to traditional fine-mesh methods.

The method presented in this work, named Modified Spectral Deterministic (MSD) [15, 14, 13, 8], was first tested in the computational modeling of one-dimensional problems and, based on the accuracy of numerical results and low execution times achieved in these simulations, we sought to extend this methodology to two-dimensional cases [13, 8], where only isotropic problems were solved. It is a coarse-mesh method that uses the intranodal analytical solution of the neutron transport equation and an iterative process to calculate the emergent neutron angular fluxes of each node that composes the discretized spatial domain. As some fixed-source problems are modelled with anisotropic physical-material parameters, an extension of this method's equations was developed and studied, in order to solve linearly anisotropic cases.

In this work, we use the discrete ordinates formulation S_N to discretize the angular variables, and the energy multigroup formulation to treat the energy variable. We consider

rectangular two-dimensional geometry and linearly anisotropic scattering cross-sections, as well as a constant approximation for the transverse neutron leakage. Here, two multigroup model-problems were solved, and precision tests were performed, comparing the numerical results obtained with the MSD-CN, the fine-mesh reference method DD, and other spectral-nodal methods from the literature.

We now present the sections comprising this comprehensive work. In Section 2, we delve into the mathematical modeling of the S_N multigroup neutron transport equation, which is applied to stationary two-dimensional fixed-source problems. Moving forward to Section 3, we show the Modified Spectral Deterministic method developed for linearly anisotropic scattering, accompanied by its local analytical solution. Advancing to Section 4, we provide an exposition of the solution to two multigroup anisotropic model-problems and compare its numerical results between fine-mesh and spectral-nodal methods from the literature. Lastly, in Section 5, we engage in a discussion of the results achieved, offering conclusions derived from this work.

2. MATHEMATICAL MODELLING

In this work, we consider the solution of fixed-source, time-independent problems in a two-dimensional Cartesian geometry domain. The neutron transport equation, considering linearly anisotropic scattering term, in the discrete ordinates formulation and the energy multigroup formulation [6], is given by [12].

$$\mu_m \frac{\partial}{\partial x}\psi_{m,g}(x,y) + \eta_m \frac{\partial}{\partial y}\psi_{m,g}(x,y) + \sigma_{T,g}(x,y)\psi_{m,g}(x,y) =$$
$$\frac{1}{4}\sum_{g'=1}^{G}\sum_{n=1}^{M}\left[\sigma_{S0}^{g'\to g}(x,y) + 3\sigma_{S1}^{g'\to g}(x,y)(\mu_m\mu_n + \eta_m\eta_n)\right]\psi_{n,g'}(x,y)\omega_n + Q_g(x,y), \qquad (1)$$
$$m = 1:M,\ g = 1:G,$$

where $\psi_{m,g}(x,y)$ represents the Angular neutron fluxes of energy group g, the macroscopic total and scattering cross sections of zero'th and first degrees from group g' to g are given respectively by $\sigma_{T,g}(x,y)$, $\sigma_{S0}^{g'\to g}(x,y)$ and $\sigma_{S1}^{g'\to g}(x,y)$, these parameters account for the probabilities of interactions between neutrons and the nuclei composing the medium. The total macroscopic cross section, $\sigma_{T,g}(x,y)$, represents the probability that a neutron undergoes any interaction per unit path length, therefore, it has units of cm^{-1}. The macroscopic scattering cross sections represent the probability per unit path length that a neutron is scattered from energy group $g'$to g, redistributing neutrons in direction and possibly in energy. The zeroth-order term describes isotropic scattering with no angular preference, while the first-order term accounts for linear angular anisotropy. The discrete angular coordinates are given by μ_m and η_m. The weights for the Level-Symmetric quadrature of order N (LQ_N) are given by ω_m. The variable $Q_g(x,y)$ represents an isotropic fixed-source, emitting neutrons of energy group g placed in (x,y). The total number of discrete directions and the number of discretized energy groups are given by M and G.

The discretization of the angular variables was made using the Level-Symmetric Quadrature of order N (LQ_N) [12]. This scheme uses a set of M discrete ordinates to describe the neutron's traveling directions $M = N(N+2)/2$, consisting in $M/4$ directions for each quadrant, as shown in Figure 1, for $N = 6$.

Figure 1:Level-Symmetric Quadrature (LQ_6)

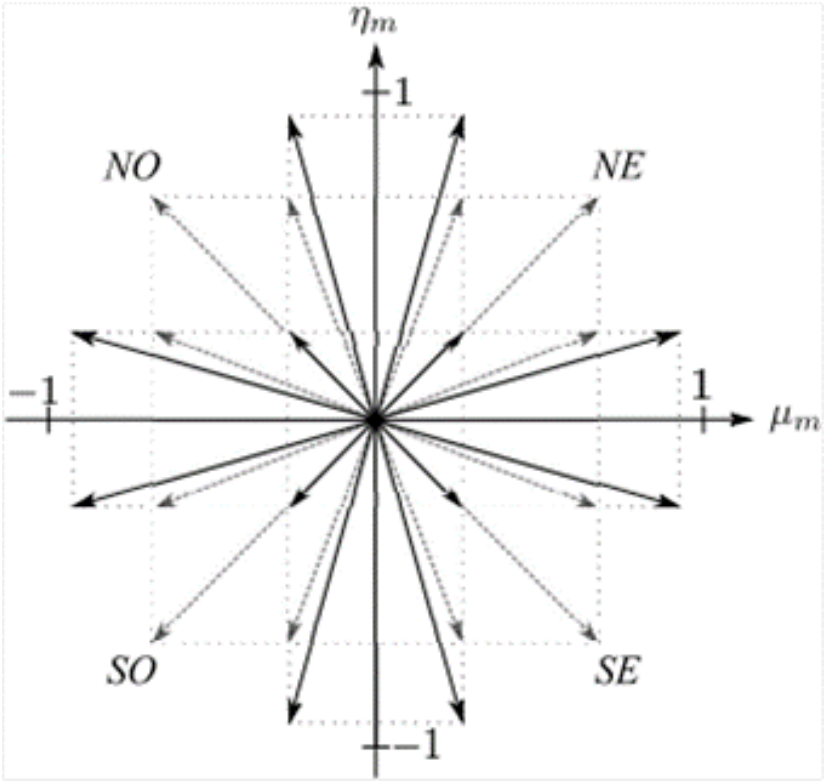

To calculate the neutron angular fluxes using nodal methods, the spatial domain needs to be partitioned into nodes. As illustrated in Figure 2, the spatial domain is partitioned into $I \times J$ nodes $\Gamma_{i,j}$, each with dimensions $[0, h_{x,i}] \times [0, h_{y,j}]$, where the coordinates within an arbitrary nodes are defined according to Figure 3. This partitioning process involves the division of the spatial domain into nodes with uniform physical-material parameters and external neutron sources.

Figure 2: Discretized Spatial Domain

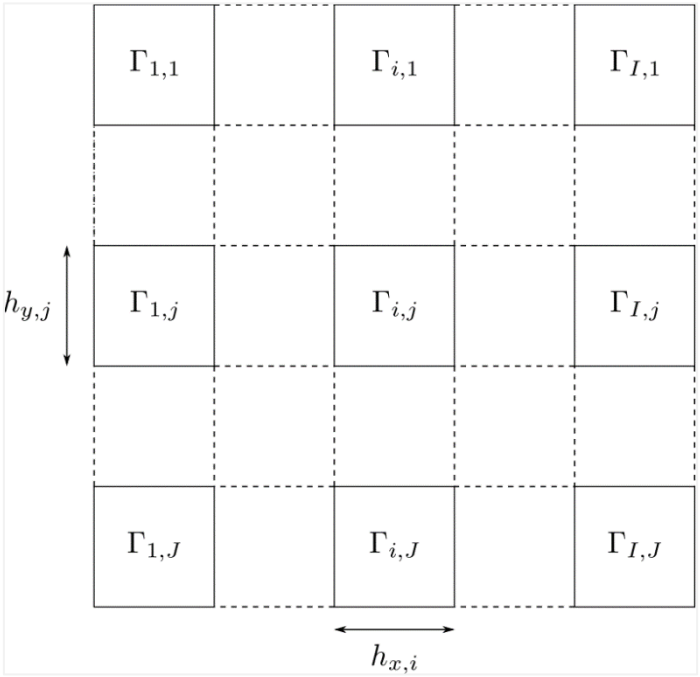

Figure 3: Spatial coordinates of the $\Gamma_{i,j}$ node

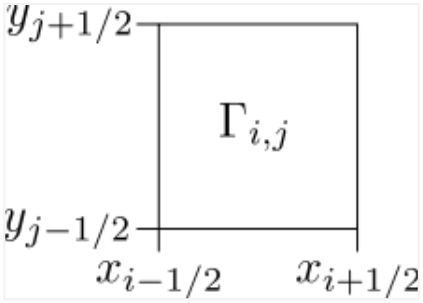

Within an arbitrary node $\Gamma_{i,j}$, we can derive the S_N intranodal neutron transport equation from Eq. (1)

$$\mu_m \frac{\partial}{\partial x}\psi_{m,g}(x,y) + \eta_m \frac{\partial}{\partial y}\psi_{m,g}(x,y) + \sigma_{T,g,i,j}\psi_{m,g}(x,y) = \frac{1}{4}\sum_{g'=1}^{G}\sum_{n=1}^{M}\left[\sigma_{S0,i,j}^{g'\to g} + 3\sigma_{S1,i,j}^{g'\to g}(\mu_m\mu_n + \eta_m\eta_n)\right]\psi_{n,g'}(x,y)\omega_n + Q_{g,i,j}, \quad (2)$$

$$m = 1:M,\ g = 1:G,\ 0 \le x \le h_{x,i},\ 0 \le y \le h_{y,j}.$$

The system of differential equations given by Eq. (2) can satisfy three types of boundary conditions (depending on the problem), namely:

- Prescribed: the values of the incoming neutron angular fluxes on the boundary of the domain are known.
- Vacuum: this boundary condition can be seen as a particular case of the prescribed one, where the incoming neutron angular fluxes on the boundaries are null.
- Reflexive: the incoming neutron angular fluxes of the boundaries are equal to the outgoing neutron angular fluxes in the same position and reflexive complementary direction.

3. MODIFIED SPECTRAL DETERMINISTIC METHOD (MSD-CN)

To derive the equations of the Modified Spectral Deterministic (MSD-CN) method [13, 8], we need to perform the transverse integration of Eq. (2) using the operator:

$$\frac{1}{h_{u,s}} \int_{u_{s-1/2}}^{u_{s+1/2}} (\cdot)\, \mathrm{d}u. \tag{3}$$

Once all steps performed in the x and y axes are analogous, the calculations will be presented only in the x axis. Thus, by applying this operator in Eq. (2) for $u = y$ and $s = j$, we obtain the transverse integrated intranodal S_N neutron transport equation in the following form:

$$\begin{aligned} &\mu_m \frac{\mathrm{d}}{\mathrm{d}x}\widetilde{\psi}_{m,g,j}(x) + \frac{\eta_m}{h_{y,j}}\left(\psi_{m,g,j+\frac{1}{2}}(x) - \psi_{m,g,j-\frac{1}{2}}(x)\right) + \sigma_{T,g.i,j}\widetilde{\psi}_{m,g,j}(x) \\ &= \sum_{g'=1}^{G}\sum_{n=1}^{M}\frac{\omega_n}{4}\left[\sigma_{S0,i,j}^{g'\to g} + 3\sigma_{S1,i,j}^{g'\to g}(\mu_m\mu_n + \eta_m\eta_n)\right]\widetilde{\psi}_{n,g'}(x) + Q_{g,i,j},\ m = 1:M,\ g = 1:G, \end{aligned} \tag{4}$$

Where $\tilde{\psi}_{m,g,j}(x)$ represents the average neutron angular fluxes transverse to the y direction, defined as

$$\widetilde{\psi}_{m,g,j}(x) \equiv \frac{1}{h_{y,j}} \int_{y_{j-\frac{1}{2}}}^{y_{j+\frac{1}{2}}} \psi_{m,g}(x,y)\mathrm{d}y.$$

The system of equations given by Eqs. (4) consists of GM equations and 2GM unknowns, half of which are the neutron angular fluxes and the other half are the transverse leakage terms described by

$$\widehat{\psi}_{m,g,i}(y) \equiv \frac{1}{h_{x,i}} \int_{x_{i-\frac{1}{2}}}^{x_{i+\frac{1}{2}}} \psi_{m,g}(x,y)\mathrm{d}x.$$

In order to match the number of equations and unknowns in this system of equations, the transverse leakage terms are approximated as constants [16], as follows:

$$\frac{\eta_m}{h_{y,j}}\left(\psi_{m,g,j+1/2(x)} - \psi_{m,g,j-1/2(x)}\right) \approx \frac{\eta_m}{h_{y,j}}\left(\widehat{\psi}_{m,g,i,j+1/2} - \widehat{\psi}_{m,g,i,j-1/2}\right) \equiv \widehat{L}_{m,g,i,j} \tag{5}$$

With these approximations, the transverse integrated S_N intranodal neutron transport equations can be rewritten as

$$\begin{aligned}&\mu_m \frac{\mathrm{d}}{\mathrm{d}x}\widetilde{\psi}_{m,g,j}(x) + \widehat{L}_{m,g,i,j} + \sigma_{T,g.i,j}\widetilde{\psi}_{m,g,j}(x) = \\ &\sum_{g'=1}^{G}\sum_{n=1}^{M}\frac{\omega_n}{4}\left[\sigma_{S0,i,j}^{g'\to g} + 3\sigma_{S1,i,j}^{g'\to g}(\mu_m\mu_n + \eta_m\eta_n)\right]\widetilde{\psi}_{n,g'}(x) + Q_{g,i,j},\ m = 1:M,\ g = 1:G,\end{aligned} \tag{6}$$

The analytical solution of the transverse-integrated S_N intranodal neutron transport equation with constant approximation in the transverse leakage terms is a combination of the homogeneous and particular solutions as $\tilde{\psi}_{m,g}(x) = \tilde{\psi}^h_{m,g}(x) + \tilde{\psi}^p_{m,g}$.

The particular solution for the x coordinate is obtained by substituting $\tilde{\psi}^p_{m,g}$ into Eq.(6), leading to the following problem:

$$\begin{aligned}&\sum_{g'=1}^{G}\sum_{n=1}^{M}\left(\sigma_{T,g,i,j}\delta_{mn}\delta_{g'g} - \frac{1}{4}\sigma_{S0,i,j}^{g'\to g}\omega_n - \frac{3}{4}\sigma_{S1,i,j}^{g'\to g}(\mu_m\mu_n + \eta_m\eta_n)\omega_n\right)\widetilde{\psi}^p_{n,g'} = \\ &Q_{g,i,j} - \widehat{L}_{m,g,i,j}.\end{aligned} \tag{7}$$

For the homogeneous component of the solution, the following expressions must be considered:

$$\widetilde{\psi}^{h}_{m,g,j}(x) = a^{x}_{m,g}(\vartheta^{x}) \exp\left(\frac{-\left(x - x_{i-1/2}\right)}{\vartheta^{x}}\right) \tag{8}$$

To calculate the homogeneous components of the solution, we substitute Eq. (8) into the homogeneous part of Eq. (6), resulting in the eigenvalue problems for the coordinate axis x:

$$\frac{1}{\mu_m}\sum_{g'=1}^{G}\sum_{n=1}^{M}\left(\sigma_{T,g,i,j}\delta_{mn}\delta_{g'g} - \frac{1}{4}\sigma^{g'\to g}_{S,i,j}\omega_n - \frac{3}{4}\sigma^{g'\to g}_{S1,i,j}(\mu_m\mu_n + \eta_m\eta_n)\omega_n\right)a^{x}_{n,g'}(\vartheta^{x}) = \frac{1}{\vartheta^{x}}a^{x}_{m,g}(\vartheta^{x}), m = 1:M, g = 1:G, \tag{9}$$

The solution of these eigenvalues problems generates a set of MG symmetric eigenvalues (ϑ^{x}) for each coordinated axis, and their corresponding eigenvectors components $a^{x}_{n,g'}(\vartheta^{x})$.

Now, the general analytical solution of the S_N transverse integrated neutron transport equation can be written respectively for x and y as

$$\widetilde{\psi}_{m,g,j}(x) = \sum_{l=1}^{GM}\alpha_l a^{x}_{m,g}(\vartheta^{x}_{l}) \exp\left(\frac{-\left(x - x_{i-\frac{1}{2}}\right)}{\vartheta^{x}_{l}}\right) + \widetilde{\psi}^{p}_{m,g}, m = 1:M, g = 1:G, \tag{10}$$

where α_l represents the eigenfunction expansion coefficients [16], which can be calculated respectively as

$$\boldsymbol{\alpha} = \sum_{l=1}^{GM}\left[a^{x}_{m,g}(\vartheta^{x}_{l}) \exp\left(\frac{-\left(x - x_{i-\frac{1}{2}}\right)}{\vartheta^{x}_{l}}\right)\right]^{-1}\left(\widetilde{\psi}_{m,g,j}(x) - \widetilde{\psi}^{p}_{m,g}\right), m = 1:M, g = 1:G, \tag{11}$$

The first step to derive the equations used in the MSD-CN's iterative process is to apply the average operator given by Eq. (3) to the intranodal neutron transport equations. For the x coordinated axis, we have

$$\frac{\mu_m}{h_{x,i,j}}(\widetilde{\psi}_{m,g,i+\frac{1}{2},j} - \widetilde{\psi}_{m,g,i-\frac{1}{2},j}) + \widehat{L}_{m,g,i,j} + \sigma_{T,g.i,j}\tau^x_{m,g,i,j} = \frac{1}{4}\sum_{g'=1}^{G}\sum_{n=1}^{M}\left[\sigma^{g'\to g}_{S0,i,j} + 3\sigma^{g'\to g}_{S1,i,j}(\mu_m\mu_n + \eta_m\eta_n)\right]\tau^x_{n,g',i,j}\omega_n + Q_{g,i,j}. \tag{12}$$

where the average neutron angular flux estimates are defined as

$$\tau^x_{m,g,i,j} \equiv \frac{1}{h_{x,i}}\int_{x_{i-\frac{1}{2}}}^{x_{i+\frac{1}{2}}} \widetilde{\psi}_{m,g,j}(x)\mathrm{d}x = \frac{1}{h_{x,i}}\sum_{l=1}^{GM}\alpha_l a^x_{m,g}(\vartheta^x_l)\left(e^{\frac{-h_{x,i}}{\vartheta^x_l}} - 1\right) + \widetilde{\psi}^p_{m,g}. \tag{13}$$

It is important to point out that during the estimates for the average neutron angular fluxes may present different values for each of the coordinated axes. Although, at the end of the iterative process execution, both $\tau^x_{m,g,i,j}$ and $\tau^y_{m,g,i,j}$ must present the same values within the precision set for the solution of the problem.

Now, the equations to iterate the neutron angular fluxes on each nodal interface can be derived. For the x coordinate axis, a few algebraic steps are performed on Eq. (12) to isolate the neutron angular fluxes on the east and west faces of $\Gamma_{i,j}$, resulting respectively in

$$\widetilde{\psi}_{m,g,i+\frac{1}{2},j} = \widetilde{\psi}_{m,g,i-\frac{1}{2},j} + \frac{h_{x,i,j}}{\mu_m}\left(-\widehat{L}_{m,g,i,j} - \sigma_{T,g.i,j}\tau^x_{m,g,i,j} + \frac{1}{4}\sum_{g'=1}^{G}\sum_{n=1}^{M}\left[\sigma^{g'\to g}_{S0,i,j} + 3\sigma^{g'\to g}_{S1,i,j}(\mu_m\mu_n + \eta_m\eta_n)\right]\tau^x_{n,g',i,j}\omega_n + Q_{g,i,j}\right),\ m = 1:M,\ g = 1:G, \tag{14}$$

The iterative process involves four sweeps throughout the domain, where each one of them calculates the emergent transverse integrated neutron angular fluxes of one quadrant for both the x and y coordinate axes. The process begins by sweeping in the SW $\to NE$ direction, which corresponds to the neutron angular fluxes of the first quadrant, as shown in Figure 4. The first spatial node to be evaluated is the bottom left one. Firstly, the transverse neutron leakage of this node is evaluated using Eq. (5). Then, with the incident transverse integrated neutron angular fluxes of $\Gamma_{i,j}$, a set of α parameters are calculated using the analytical solution of the intranodal S_N neutron transport equation. On the next step, Eq. (12) calculates estimates for the outgoing average neutron angular fluxes. Finally, after these

steps, the emergent transverse integrated neutron angular fluxes of the first node can be calculated using Eq. (14) for the first quadrant, where $\mu_n > 0$ and $\eta_n > 0$. To show the position of these fluxes inside the node, they are represented in Figure 4 as dashed red arrows.

The initial spatial grid is illustrated in Figure 5 as an example with 6 nodes. The transverse integrated neutron angular fluxes estimates are shown as dotted grey arrows, while the boundary conditions are shown as the black arrows.

Figure 4: Neutron angular fluxes within a spatial node $\Gamma_{i,j}$

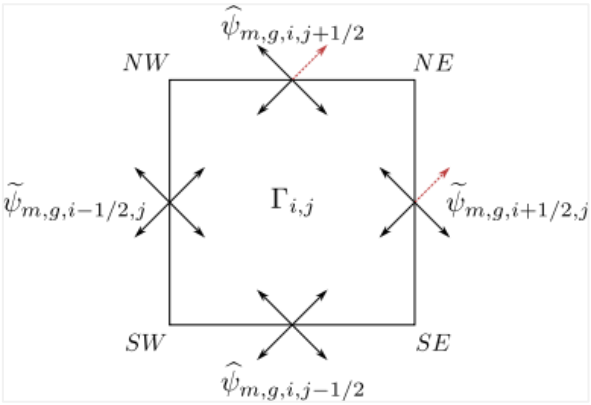

Figure 5: Initial iteration scheme

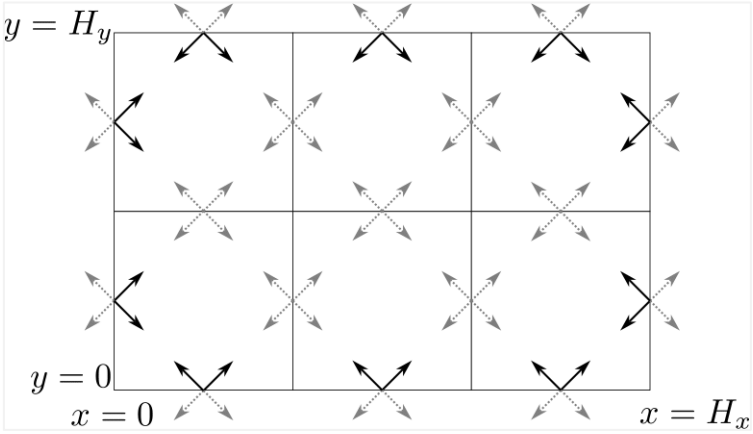

The emergent transverse integrated neutron angular fluxes of the first node are now updated through the iterative process, resulting in new estimates shown in Figure 7 as the red dashed arrows.

The same process is then repeated for the entire domain, calculating the emergent transverse integrated neutron angular fluxes of the first quadrant. After completing the first sweep, the second sweep starts using the same steps as before but, in the direction, SE $\rightarrow$ *NW* ($\mu_n < 0$ and $\eta_n > 0$), beginning at the rightmost bottom node. By calculating the emergent transverse integrated neutron angular fluxes of this first node, the domain is updated and arranged as shown in Figure 7.

Figure 6: Iterated outgoing neutron angular fluxes of the first node.

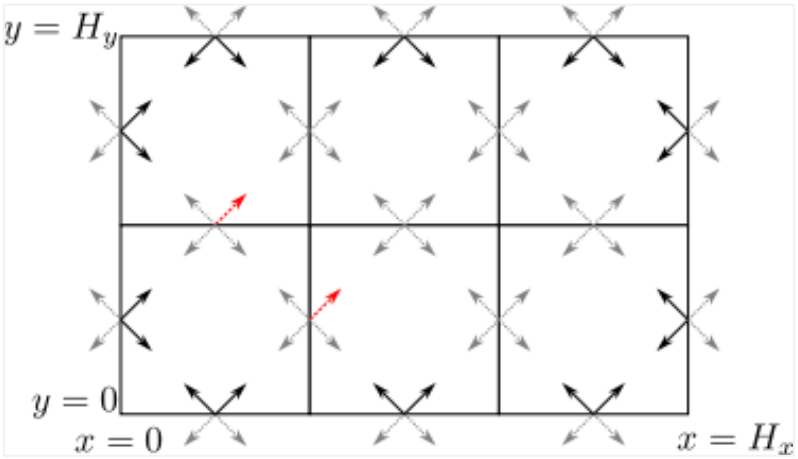

Figure 7: First sweeping direction completed.

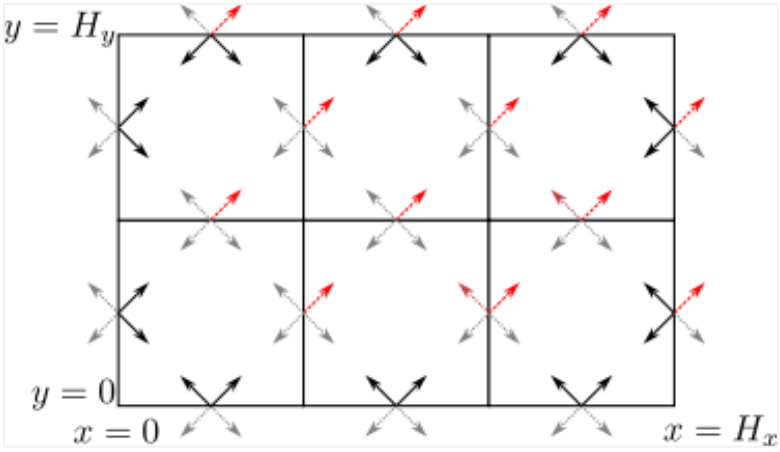

The steps above are repeated for all nodes $\Gamma_{i,j}$ in the domain, resulting in the calculation of the emergent transverse integrated neutron angular fluxes in all 4 quadrants for each node.

Several stopping criteria can be used to determine when to end an iteration. In this work, the average neutron scalar flux is used as the criterion. It is calculated in each node as follows:

$$\overline{\phi}_{g,i,j}^{u\,(k)} = \frac{1}{4}\sum_{n=0}^{M}\omega_n \tau_{n,g,i,j}^{u\,(k)},\ u = x,\ y. \tag{15}$$

The parameter k represents the iteration number. To determine when the iterative process should be stopped, the maximum standard deviation between the average neutron scalar flux of each node $\Gamma_{i,j}$ from two consecutive iterations is compared against a given precision ξ. The stopping criterion can be expressed as follows:

$$\underset{g,i,j,u}{\text{MAX}} \left| \frac{\overline{\phi}_{g,i,j}^{u\,(k)} - \overline{\phi}, y_{g,i,j}^{u\,(k-1)}}{\overline{\phi}_{g,i,j}^{u\,(k-1)}} \right| < \xi \tag{16}$$

4. NUMERICAL RESULTS

In this section, we present the numerical results of two model problems and compare the accuracy of the Modified Spectral Deterministic (MSD-CN) method [14, 13, 15, 8] using different meshes and quadrature orders. The reference method used for all the model problems is the fine-mesh Diamond Difference (DD) method [12]. We also compared the numerical results obtained with the MSD-CN and the nodal method MR-CN [9,20]. Alongside the precision test, a performance test was also executed, comparing the average execution time of multiple executions of the SDM-CN and DD methods.

To create the mesh, we divided the spatial domain into J_x nodes along the x coordinate axis and J_y nodes along the y coordinate axis, resulting in a total of $J_x \times J_y$ nodes throughout the domain $[0, H_x] \times [0, H_y]$. The meshes used for the fine-mesh reference were refined until no differences were seen within the number of decimal places studied for the

analyzed quantity of the model-problem. All methods were developed using the C++ programming language, and for solving the eigenvalue problem in the MSD-CN the Alglib [7] library was used. The MSD-CN and DD methods were executed on a computer with an AMD Ryzen 7 3700U processor and 12 Gb of RAM.

4.1. Model-Problem 1

The first model-problem studied in this work consists in the shielding of a neutron source, originating due to spallation reactions. This problem was adapted using 4 energy group data of the ADS reactor core present in [22], who kindly provided the physical-material data obtained with the *OpenMC* code. The physical-material parameters of zones 1, 2, and 3, shown in Figure 8, are respectively the same Spallation Target, LBE Buffer, and SUS B_4C shield regions present in [22]. The geometry, dimensions, and boundary conditions of this problem are shown in Figure 8.

It is important to note that the neutron source resides evenly throughout Zone 1, where high energy protons collide with the Lead-Bismuth target producing neutrons, surrounded by a buffer and a reflector layer, adapted from, where the physical-material parameters for all regions were obtained in [22]. In this representation, the innermost region, named 1, is the Pb-Bi spallation target, region 2 is a layer of buffer which may decrease the spallation neutron source, and the outermost region is a reflective layer.

The physical-material parameters of the material zones are modelled with 4 energy groups, shown in the annex 1, respectively for the Reflector, Buffer and Pb-Bi neutron spallation Target.

Figure 8: Model-problem 1.

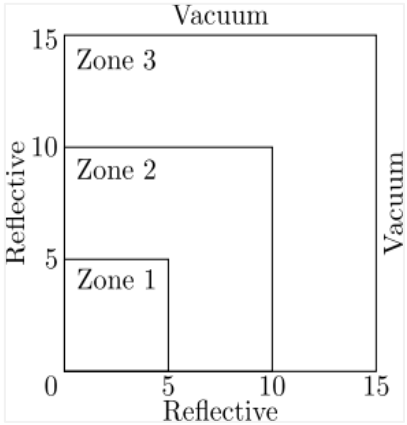

This problem was solved using S_4 and S_8 Level Symmetric quadrature, with $\xi = 10^{-5}$ precision. The mesh used in the fine-mesh reference was composed of 100 nodes in $[0, 5]$, 200 nodes in $[5, 10]$ and 300 in $[10, 15]$, on both the x and y axes. The selection of this mesh, with a larger quantity of nodes on the outermost regions, is because numerical results tend to have larger deviations as it gets further from the neutron source, once it tends to have smaller values for the neutron angular fluxes. Together with this, a coarse approximation was used for the transverse neutron leakage term (constant approximation), which could lead to numerical results with higher deviation when compared to a fine-mesh reference. Thus the numerical results could benefit from a finer mesh near the vacuum boundaries.

For this case, the net neutron leakage on the east boundary of the spatial domain was calculated according to the form:

$$F_{x,g}^{+} = \sum_{j=1}^{J_y} h_{y,j} \left(\sum_{n=1}^{M/4} \omega_n \mu_n \overline{\psi}_{x,n,g}^{i,j}(H_x) + \sum_{n=3M/4+1}^{M} \omega_n \mu_n \overline{\psi}_{x,n,g}^{i,j}(H_x) \right) \tag{17}$$

The results are displayed in Tables 1 and 2, where this variable is shown for each one of the 4 energy groups, and the relative percentual deviation between the fine-mesh reference, and MSD-CN or RM-CN is shown inside the parenthesis. A set of 3 spatial grids

was tested following the same proportion of the reference grid, with k divisions in the target, $2k$ divisions in the buffer and $3k$ in the reflector along each coordinated axis.

Table 1: Net neutron leakage [$cm^{-2}s^{-1}$] - Model-problem 1 - S_4

Method	Mesh	g = 1	g = 2	g = 3	g = 4
DD	600 × 600	1.2311e+01 [1]	1.2557e+01	1.2097e+01	1.9896e+00
MSD-CN	6 × 6	1.2310e+01 (0.0081%) [2]	1.2553e+01 (0.0318%)	1.2093e+01 (0.0330%)	1.9917e+00 (0.1055%)
	12 × 12	1.2310e+01 (0.0081%)	1.2556e+01 (0.0079%)	1.2096e+01 (0.0082%)	1.9909e+00 (0.0653%)
	24 × 24	1.2311e+01 (0.0000%)	1.2557e+01 (0.0000%)	1.2097e+01 (0.0000%)	1.9910e+00 (0.0703%)
RM-CN	6 × 6	1.2310e+01 (0.0081%)	1.2553e+01 (0.0318%)	1.2092e+01 (0.0413%)	1.9912e+00 (0.0804%)
	12 × 12	1.2310e+01 (0.0081%)	1.2556e+01 (0.0079%)	1.2096e+01 (0.0082%)	1.9909e+00 (0.0653%)
	24 × 24	1.2311e+01 (0.0000%)	1.2557e+01 (0.0000%)	1.2097e+01 (0.0000%)	1.9909e+00 (0.0653%)

[1] Read as 1.2311×10^{1} $cm^{-2}s^{-1}$

[2] Percentage Standard Deviation between SDM and DD as $|SDM - DD|/DD \times 100\%$.

The results obtained in this study showed that the MSD-CN was able to compute accurate results for this case even with the coarser mesh used, having the largest deviation being lower than 0.11 %. For the finer mesh used in the spectral-nodal methods (24×24), reached the exact result, within the considered decimal places, when compared to the reference for the first 3 energy groups, and a deviation smaller than 0.08 % in for the neutron leakage in $g = 4$.

Table 2: Net neutron leakage [cm-2s-1] - Model-problem 1 – S_8

Method	Mesh	g = 1	g = 2	g = 3	g = 4
DD	300 × 300	1.2272e+01 [1]	1.2516e+01	1.2075e+01	1.9852e+00
MSD-CN	6 × 6	1.2268e+01 (0.0325%) [2]	1.2511e+01 (0.0399%)	1.2071e+01 (0.0331%)	1.9872e+00 (0.1007%)
	12 × 12	1.2272e+01 (0.0000%)	1.2515e+01 (0.0080%)	1.2074e+01 (0.0083%)	1.9865e+00 (0.0654%)
	24 × 24	1.2272e+01 (0.0000%)	1.2516e+01 (0.0000%)	1.2075e+01 (0.0000%)	1.9866e+00 (0.0705%)
RM-CN	6 × 6	1.2268e+01 (0.0325%)	1.2511e+01 (0.0399%)	1.2070e+01 (0.0414%)	1.9868e+00 (0.0805%)
	12 × 12	1.2272e+01 (0.0000%)	1.2515e+01 (0.0080%)	1.2074e+01 (0.0083%)	1.9865e+00 (0.0654%)
	24 × 24	1.2272e+01 (0.0000%)	1.2516e+01 (0.0000%)	1.2075e+01 (0.0000%)	1.9866e+00 (0.0705%)

The achieved results when solving the first model-problem using S_8 Level Symmetric quadrature had good accuracy. Within all tested spatial grid meshes, the results reached with around 0.1 % or smaller deviation when compared to the fine-mesh reference. In this case, both MSD-CN and RM-CN achieved the same numerical results within the 4 decimal places studied, where the exact answer was reached in 3 of the 4 energy groups when used the 24×24 nodes mesh.

A performance test was executed, to test the execution time of the SDM-CN algorithm and compare it to the DD execution time. Multiple executions were performed to achieve an average execution time for the algorithm using each set of mesh and quadrature degree. Table 3 displays the numerical results for this test.

Table 3: Model-problem 1 – Performance test

Method	Mesh	S_4		S_8	
		Iterations	Execution time (s)	Iterations	Execution time (s)
DD	600 × 600	313	1518,592	-	-
	300 × 300	-	-	312	1586,779
SDM-CN	6 × 6	1027	2,92	1003	21,674
	12 × 12	1798	15,695	1727	139,47
	24 × 24	2325	74,65	2214	689,541

As seen in Table 3, for the S_4 case, the reference method performed its calculations for this set of parameters within 1518 seconds, while the SDM-CN reached less than 0.1 % deviation on the numerical results with less than 3 seconds of execution time, when used the 6 × 6 mesh, leading to an execution time 99% smaller than the reference. For the S_8 case, a similar behavior was achieved, where the DD method was executed within 1586 seconds, while the finest mesh of the SDM-CN was executed in less than a half of this time, reaching the same numerical results as the reference in 3 of the tested energy groups.

4.2 Model-Problem 2

The second model-problem consists in the shielding of a neutron source using two layers of shielding, adapted from [20]. The media is composed of three distinct material zones, and its physical-material parameters were provided by [11]. The total macroscopic cross-section of each material zone and energy group is given by:

$$\sigma_{T,g,z} = \left(\frac{z+20}{21}\right)^5 \left(\frac{g}{10} - 0.15\delta_{5,g} - 0.15\delta_{10,g}\right) \ cm^{-1}, g = 1:10. \tag{18}$$

The macroscopic scattering cross-sections of the material zone z from group g' to g of l'th order are given by

$$\sigma_{Sl,z}^{g'\to g} = \left(\frac{z+20}{21}\right)\left(\frac{g'}{100(g-g'+1)}\right)\left(0.7 - \frac{g+g'}{200}\right)^l \ cm^{-1}, g = 1:10, \ l = 0:1. \tag{19}$$

The modelled domain is a square of size $25 \times 25\ cm^2$, as illustrated in Figure 9, where the boundary conditions are also displayed. The neutron source is in the same region as material zone 1, and is defined as follows:

$$Q_g = (1.1 - 0.1g),\ g = 1 : 10. \tag{20}$$

In this case, we analyze the response of a detector D with dimensions of $2 \times 2\ cm^2$, which is placed in the top right corner of the domain. To calculate the absorption rate density in group g for the nodes $\Gamma_{i,j}$ within the detector D, we use the following equation:

$$T_{g,i,j} = \sum_{i=I_x}^{I} \sum_{j=J_y}^{J} \sigma_{a,g,i,j} \overline{\phi}_{g,i,j} h_{x,i} h_{y,j}, \tag{21}$$

where $\sigma_{a,g,i,j}$ represents the macroscopic absorption cross-section, calculated as

$$\sigma_{a,g,i,j} = \sigma_{T,g,i,j} - \sum_{g'=1}^{G} \sigma_{S0,i,j}^{g \to g'}, \tag{22}$$

and the indexes $[J_x, J] \times [J_y, J]$ represents the nodes $\Gamma_{i,j}$ within the detector D.

A reference calculation was performed using the DD method with a 500 × 500 node mesh. We then compared the absorption rate densities of energy groups 1, 5, and 10 obtained with the MSD-CN using 3 different sets of mesh and the reference results, using a quadrature order of LQ_4 in the form of a percentage relative deviation. A comparison between the results obtained with the RM-CN and the reference was also made. All these results are displayed in Table 3.

Figure 9: Model-problem 2 geometry

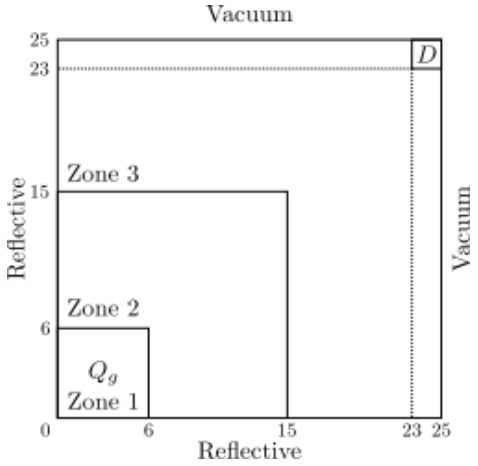

Table 4: Absorption rate density [absorptions/s] in D detector - Model-problem 2.

Method	Mesh	g = 1	g = 5	g = 10
DD	500 × 500	5.7585×10^{-4}	1.2405×10^{-5}	7.0987×10^{-6}
MSD-CN	25 × 25	5.9678×10^{-4} (3.6346%) [2]	1.2959×10^{-5} (4.4594%)	7.5027×10^{-6} (5.6911%)
	50 × 50	5.8799×10^{-4} (2.1088%)	1.2495×10^{-5} (0.7230%)	7.1905×10^{-6} (1.2936%)
	75 × 75	5.7645×10^{-4} (0.1057%)	1.2419×10^{-5} (0.1085%)	7.1149×10^{-6} (0.2284%)
RM-CN	25 × 25	5.9678×10^{-4} (3.6346%)	1.2959×10^{-5} (4.4594%)	7.5027×10^{-6} (5.6911%)
	50 × 50	5.8800×10^{-4} (2.1099%)	1.2493×10^{-5} (0.7093%)	7.1893×10^{-6} (1.2762%)
	75 × 75	5.7645×10^{-4} (0.1057%)	1.2419×10^{-5} (0.1085%)	7.1150×10^{-6} (0.2296%)

A decreasing percentage relative deviation is obtained as the number of nodes is increased in the mesh, analyzing the numerical results of this behavior in present in both MSD-CN and RM-CN. Using a mesh with 75×75 nodes, the MSD-CN showed the largest deviation, which was 0.2284 %, in the tenth group. Considering that results tend to have higher deviations in regions that are farther from external sources, as observed in model-problem 1, we can conclude that the MSD-CN was able to solve this model-problem accurately for the tested meshes. When comparing both coarse-mesh methods, it can be seen little to no deviations among its numerical results within the precision studied in this model-problem.

A performance test similar to the previous case was also performed in this model-problem, with numerical results displayed in Table 5.

Table 5: Model-problem 2 performance test

Method	Mesh	S_4	
		Iterations	Execution time (s)
DD	500 × 500	23	120,15
SDM-CN	25 × 25	1029	202,192
	50 × 50	1171	913,579
	75 × 75	2002	6345,897

In this model problem, even on the first mesh tested, the SDM-CN exhibited execution times higher than those of the fine-mesh reference. Consequently, further studies indicate that optimization strategies, such as parallelization of the iterative solver, could be a way to combine the low deviations achieved by the method with improved computational performance.

A better overview of the absorption rate density across all spatial domain is shown in Figures 10-15. As the average absorption rate density is uniform within the nodes, a bar three-dimensional bar chart fits adequately to represent each of the nodes in the $x - y$ plane and the absorption rate density as a bar in the z axis. Among these figures, it is displayed the results obtained for energy groups 1, 5 and 10, as analyzed in the tables, with a 75×75 mesh for the MSD and 200×200 mesh for the DD.

Figure 10: Absorption rate density - MSD-CN - $g = 1$

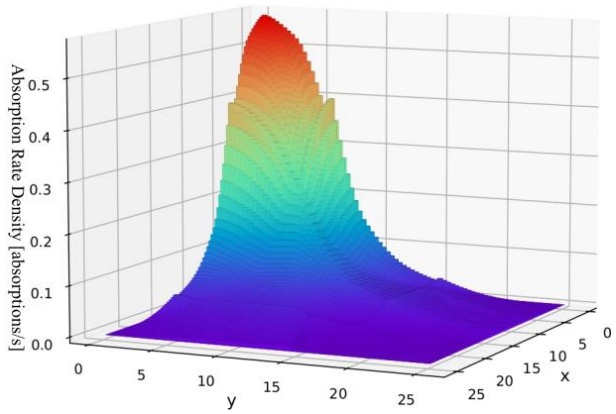

Figure 11: Absorption rate density- DD - $g = 1$

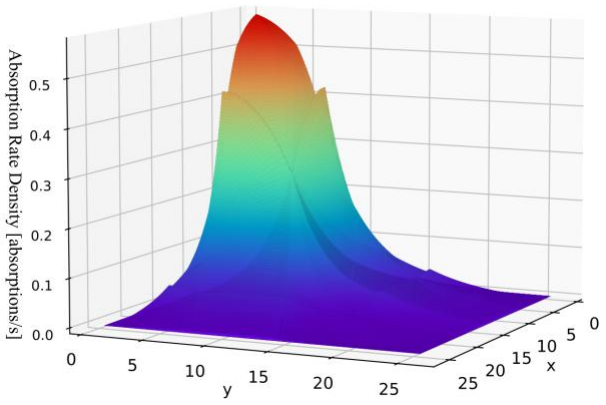

Figure 12: Absorption rate density- MSD-CN – $g = 5$

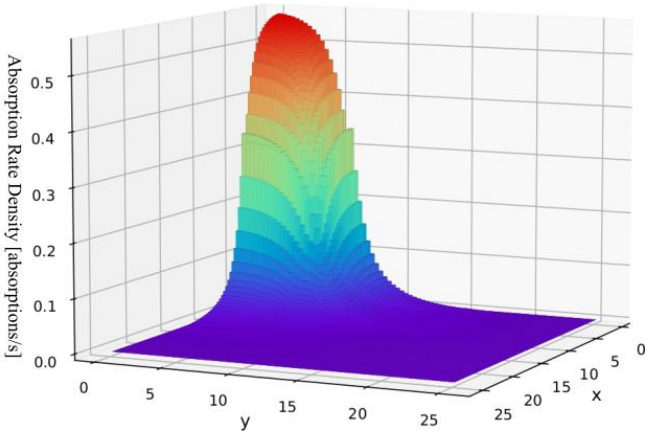

Figure 13: Absorption rate density - 3 DD – $g = 5$

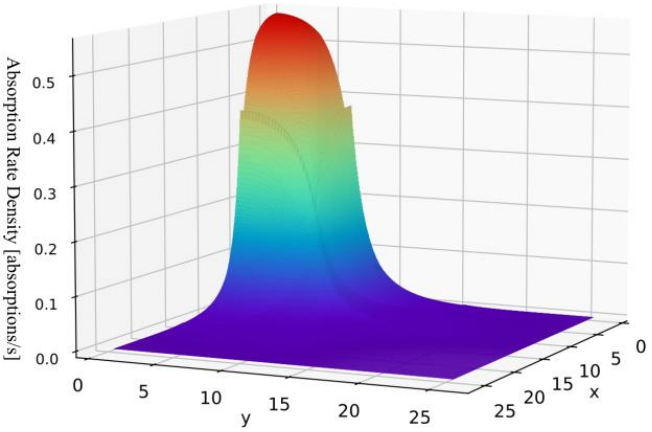

Figure 14: Absorption rate density - MSD-CN - $g = 10$

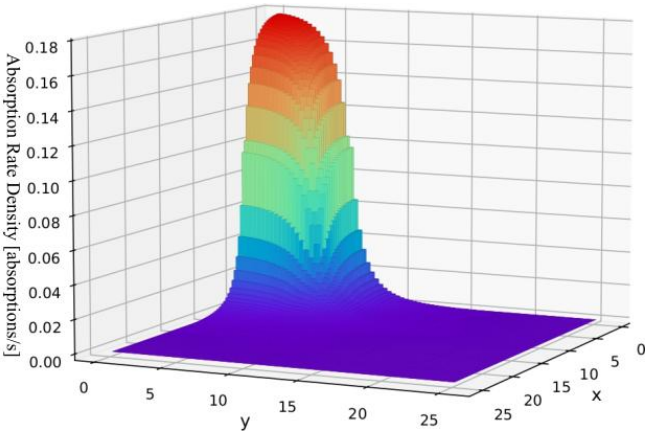

Figure 15: Absorption rate density - DD - $g = 10$

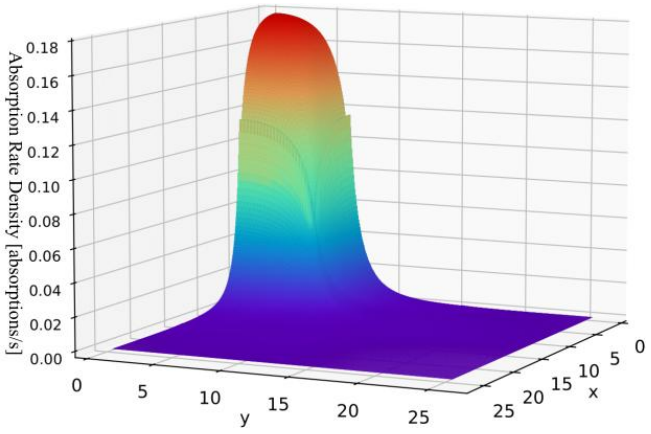

A reasonable behavior was achieved when generating these results, once the absorption rate density has higher values within the neutron source, being $[0,6] \times [0,6]$ and decreasing along the domain as it gets further from the source, with symmetrical results between the x and y axes. When comparing the results between the MSD-CN and DD, it can be seen a very similar behavior of the absorption rate density along all spatial domain in all energy groups.

5. CONCLUDING REMARKS

In this work, we presented an extension of the coarse-mesh method named Modified Spectral Deterministic [15, 13, 14] to solve fixed-source problems considering linearly anisotropic scattering. In this method, the outgoing neutron angular fluxes are calculated in an iterative process, using the nodal balance equation, as seen in the fine-mesh method Diamond Difference [12]. We solved a set of two model-problems and compared their precision with fine and coarse-mesh methods found in the scientific literature, while assuming a constant approximation for the transverse neutron leakage.

The first model-problem consists in the shielding of the Pb-Bi target, surrounded by a buffer and a reflector layer, with physical-material parameters modelled in 4 energy groups. In this case, the neutron net leakage in the left boundary of the spatial domain is compared again between the spectral-nodal methods MSD-CN and RM-CN and the DD reference. In this model-problem, the MSD-CN and RM-CN achieved results with less than 0.12% deviation in all tested cases. Even using the coarser mesh, being 6×6, they could reach accurate results for both S_4 and S_8 quadrature orders. The performance test for this model-problem showed a decrease in the execution time, when compared to the fine-mesh reference in all tested meshes, reaching up to more than 99% execution time when used the 6×6 mesh.

In the second model-problem solved in this work, an idealized neutron shielding case is studied, with physical-material parameters discretized in 10 energy groups. In this model-

problem, the numerical results for the neutron absorption rate density in a detector located in the outermost corner of the spatial domain are compared between the MSD-CN, RM-CN and a fine-mesh reference, the DD method. Three spatial node meshes were studied, where both spectral-nodal methods achieved similar results within the 4 decimal places studied. In the finest mesh tested, the MSD-CN reached numerical results with less than 0.3% deviation among all energy groups when compared to the reference method. Unlike the first model-problem, the performance test displayed higher execution times for the SDM-CN when compared to the DD method in all tested meshes. Therefore, optimization techniques will be part of future works regarding the proposed methodology, such as the parallelization of the iterative process.

As part of future work, our group intends to develop higher-order approximations for the transverse neutron leakage, in order to enable the solution of these problems with coarser meshes, leading to more accurate deviations and smaller execution times.

ACKNOWLEDGMENTS

The authors thank the Multi-scale Particle Transport Laboratory (LABTRAN) at IPRJ/UERJ for technical support.

FUNDING

This study was financed in part by the Coordenação de Aperfeiçoamento de Pessoal de Nível Superior – Brasil (CAPES) – Finance Code 001. Rafael Libotte is supported by a doctoral fellowship from the Carlos Chagas Filho Foundation for Supporting Research in the State of Rio de Janeiro, Grant No. E-26/201.278/2023.

CONFLICT IF INTEREST

All authors declare that they have no conflicts of interest.

REFERENCES

[1] Barichello, L. B., Cabrera, L. C., Prolo Filho, J. F. An analytical approach for a nodal scheme of two-dimensional neutron transport problems. Annals of Nuclear Energy, [Publisher Location not specified], v. 38, n. 6, p. 1310–1317, 2011.

[2] Barichello, L. B., Pazinatto, C. B., Rui, K. An analytical discrete ordinates nodal solution to the two-dimensional adjoint transport problem. Annals of Nuclear Energy, [sl.l], v. 135, n. 0, p. [s.l], 2020

[3] Barros, R. C. A spectral-nodal method for the solution of discrete ordinates problems in one and two-dimensional Cartesian geometry. In: University of Michigan. Tese de Doutorado, University of Michigan, 1990.

[4] Barros, R. C., Larsen, E. W. A spectral nodal method for one-group x, y-geometry discrete ordinates problems. Nuclear Science and Engineering, [Publisher Location not specified], v. 111, n. 1, p. 34–45, 1992.

[5] Barros, R. C., Yavuz, M., Abreu, M. P., Alves Filho, H., Mello, J. A. M. Progress in spectral nodal methods applied to discrete ordinates transport problems. Progress in Nuclear Energy, [Publisher Location not specified], v. 33, n. 1–2, p. 117–154, 1998.

[6] Bell, G. I., Glasstone, S. Nuclear Reactor Theory. 2ª ed. Washington, DC: Krieger Pub Co., 1970.

[7] Bochkanov, S. Alglib. Disponível em: www.alglib.net. Acesso em: [Data de acesso não especificada].

[8] Curbelo, J. P., Libotte, R. B., Barros, R. C., Alves Filho, H. The modified spectral deterministic method applied to fixed–source discrete ordinates problems in x,y–geometry. Brazilian Journal of Radiation Sciences, [Publisher Location not specified], v. 8, n. 3A, p. [não especificado], 2020.

[9] Silva, O., Guida, M., Alves Filho, H., Barros, R. C. A response matrix spectral nodal method for energy multigroup x,y-geometry discrete ordinates problems in non-

multiplying media. Annals of Nuclear Energy, [Publisher Location not specified], v. 125, p. 1-9, 2020.

[10] Duderstadt, J. J., Hamilton, L. J., et al. Nuclear Reactor Analysis. New York, USA: Wiley, 1976.

[11] Garcia, R. D. M., Siewert, C. E. Multislab multigroup transport theory with L-th order anisotropic scattering. Journal of Computational Physics, [Publisher Location not specified], v. 50, n. 2, p. 181–192, 1983. ISSN 0021-9991.

[12] Lewis, E. E., Miller, W. F. Computational Methods of Neutron Transport. 2ª ed. New York, USA: Wiley, 1993.

[13] Libotte, R. B. Método de malha grossa para solução numérica de problemas de blindagem de nêutrons em geometria unidimensional na formulação de ordenadas discretas com perspectivas a cálculos multidimensionais em geometria retangular. Dissertação de Mestrado, Rio de Janeiro State University, 2021. (Em português)

[14] Libotte, R. B., Alves Filho, H., Barros, R. C. A novel coarse-mesh method applied to neutron shielding problems using the multigroup transport theory in discrete ordinates formulations. Brazilian Journal of Radiation Sciences, [Publisher Location not specified], v. 8, n. 3A, p. [não especificado], 2020a.

[15] Libotte, R. B., Alves Filho, H., Barros, R. C. Recent advances in a methodology for x-y Cartesian geometry neutron transport problems in non-multiplying media using the multigroup discrete ordinates formulation. In: Encontro Nacional de Modelagem Computacional, 2020. [Documento completo], [Publisher Location not specified], 2020b.

[16] Oliva, A. M. Método espectral determinístico para a solução de problemas de transporte de nêutrons usando a formulação das ordenadas discretas. Tese de Doutorado, Rio de Janeiro State University, 2018. (Em português)

[17] Oliva, A. M., Alves Filho, H., M. D., J., R., G. C. The spectral nodal method applied to multigroup sn neutron transport problems in one-dimensional geometry with fixed–source. Progress in Nuclear Energy, [Publisher Location not specified], v. 105, n. 0, p. 106–113, 2018.

[18] Picoloto, C. B., Cunha, R. D., Barros, R. C., Barichello, L. B. An analytical approach for solving a nodal formulation of two-dimensional fixed-source neutron transport problems with linearly anisotropic scattering. Progress in Nuclear Energy, [Publisher Location not specified], v. 98, n. 0, p. 193–201, 2017.

[19] Salas, L. L., Silva, F. C., Martinez, A. S. A new point kinetics model for ADS-type reactor using the importance. Annals of Nuclear Energy, [Publisher Location not specified], v. 190, n. 109869, p. 1–11, 2023.

[20] Silva, O. P. Um método de matriz resposta para cálculos de transporte multigrupos de energia na formulação de ordenadas discretas em meios não-multiplicativos. Tese de Doutorado, Rio de Janeiro State University, 2018. (Em português)

[21] Spanier, J., Gelbard, E. M. Monte Carlo Principles and Neutron Transport Problems. Courier Corporation, 2008.

[22] Tsujimoto, K., Sasa, T., Nishihara, K., Oigawa, H., Takano, H. Neutronics design for lead-bismuth cooled accelerator-driven system for transmutation of minor actinides. Journal of Nuclear Science and Technology, [Publisher Location not specified], v. 41, n. 1, p. 21–36, 2004.

LICENSE

ANNEX 1

In this annex, the physical-material Properties of the model-problem 1 are presented.

Zone 1

	g = 1	g = 2	g = 3	g = 4
$\sigma_{T,g}$	1.66467556e-01	2.07086789e-01	3.01415492e-01	3.19327346e-01

$$\sigma_{S0}^{g' \to g}$$

g'	g = 1	g = 2	g = 3	g = 4
1	1.62229135e-01	0	0	0
2	3.66970175e-03	2.05934241e-01	0	0

g'	g = 1	g = 2	g = 3	g = 4
3	4.87154527e-04	1.04883871e-03	3.01101715e-01	0
4	7.89646547e-06	0	2.01613012e-04	3.19024465e-01

$$\sigma_{S1}^{g' \to g}$$

g'	g = 1	g = 2	g = 3	g = 4
1	3.81626626e-02	0	0	0
2	-4.16075313e-04	2.03165432e-02	0	0
3	-5.83108236e-06	-3.25866705e-04	1.14221028e-02	0
4	1.09560796e-06	0	-7.00990459e-05	3.06561176e-03

Zone 2

	g = 1	g = 2	g = 3	g = 4
$\sigma_{T,g}$	2.14537815e-01	2.55923664e-01	3.67323691e-01	7.30853725e-01

$$\sigma_{S0}^{g' \to g}$$

g'	g = 1	g = 2	g = 3	g = 4
1	2.01538355e-01	0	0	0
2	1.07076213e-02	2.51286952e-01	0	0
3	1.70399299e-03	4.27683896e-03	3.65134724e-01	0
4	1.03408158e-04	9.54151640e-07	1.58064358e-03	7.28713421e-01

$$\sigma_{S1}^{g' \to g}$$

g'	g = 1	g = 2	g = 3	g = 4
1	4.84780953e-02	0	0	0
2	-1.15828648e-03	2.70259680e-02	0	0
3	2.55985043e-05	-1.21654324e-03	1.28296826e-02	0
4	4.34227123e-07	1.27920987e-08	-4.52058713e-04	8.85041993e-03

Zone 3

	g = 1	g = 2	g = 3	g = 4
$\sigma_{T,g}$	2.58411776e-01	4.02420284e-01	5.09556288e-01	6.79059327e-01

$$\sigma_{S0}^{g' \to g}$$

g'	g = 1	g = 2	g = 3	g = 4
1	2.25491340e-01	0	0	0
2	2.77092827e-02	3.54356869e-01	0	0
3	6.19818871e-04	3.48065235e-02	4.71514799e-01	0
4	3.57420692e-05	0	8.02003220e-03	5.89532641e-01

$$\sigma_{S1}^{g' \to g}$$

g'	g = 1	g = 2	g = 3	g = 4
1	4.86421427e-02	0	0	0
2	-5.31328963e-03	4.81904749e-02	0	0
3	1.61716787e-05	-1.04851793e-02	2.57298087e-02	0
4	6.61901510e-07	0	-2.48559277e-03	2.33066025e-02